Breaking time reversal symmetry by viscous dephasing

Bruno Eckhardt and Erwan Hascoët
Fachbereich Physik, Philipps Universität Marburg, D-35032 Marburg, Germany
(Received 11 April 2005; published 12 September 2005)

We show that in generic situations a reversible periodic driving of a Stokes flow will not result in a reversible flow field. Each eigenmode of the Stokes operator responds with a phase delay that depends on frequency and damping, resulting in a viscous dephasing that destroys time reversal symmetry and hence prepares for chaotic advection. The general theory is illustrated for a two-dimensional vortex pattern that can be generated in current driven flows in a magnetic field.

DOI: 10.1103/PhysRevE.72.037301 PACS number(s): 47.52.+j, 05.45.−a

I. INTRODUCTION

Reversibility of low Reynolds number flows can be impressively demonstrated with a setup introduced and popularized by G. I. Taylor [1]: a blob of dye is introduced in a narrow gap between two concentric cylinders and then stretched to near invisibility by the rotation of the inner cylinder. When the rotation is reversed, the blob reforms almost perfectly. This feature of low Reynolds number flows is generally accepted and hence avoided in systems designed to study chaotic advection [2–10]. However, the Lorenz-force driven systems used by Gollub *et al.* [11–13] seem to defy this principle: they are driven by periodic currents but nevertheless show chaotic particle advection. So how is reversibility broken?

A natural candidate for reversibility breaking is the nonlinearity, with its quadratic dependence on the velocity field. However, even if this term remains small and can be neglected, a reversible driving need not lead to a reversible response. We verify this with a decomposition of the velocity field and the spatial dependence of the driving force in terms of eigenmodes of the Stokes equation. As we will show, eigenmodes excited by the external force follow the force with a specific time delay that depends on frequency and damping rate. Thus if several modes are excited they will show different delays and this difference destroys reversibility. Time reversibility thus is lost by a *viscous dephasing* between the different Stokes modes.

II. CHARACTERISTIC SCALES

The experiments [11–13] deal with a two-dimensional (2D) flow, but the phenomenon is more general and can occur also in 3D situations. What is significant is that the flow be driven by volume forces that set the scale for the fluid response. Imagine then a flow driven by some kind of external volume force, e.g., a pressure gradient or the Lorentz force in the 2D experiments. In the Navier-Stokes equation such a forcing can be captured by a divergence-free volume force,

$$\partial_t \mathbf{u} + (\mathbf{u}\cdot\boldsymbol{\nabla})\mathbf{u} = -\boldsymbol{\nabla} p + \nu\Delta\mathbf{u} + \mathbf{f}(\mathbf{r},t). \tag{1}$$

A typical forcing is

$$\mathbf{f}(\mathbf{r},t) = f_0 \mathbf{f}(\mathbf{r}) e^{i\omega t}, \tag{2}$$

with amplitude f_0, spatial dependence $\mathbf{f}(\mathbf{r})$, and a periodic time dependence, $\exp(i\omega t)$. If imaginary parts are taken, the time-dependence of the driving becomes $\sin \omega t$ and has the symmetry

$$\mathbf{f}(-t) = -\mathbf{f}(t). \tag{3}$$

If the flow inherits this symmetry, perhaps with respect to another zero in time t_0, i.e., if

$$\mathbf{u}(t-t_0) = -\mathbf{u}(-(t-t_0)), \tag{4}$$

then advected particles reverse their paths, $\mathbf{x}(t-t_0) = -\mathbf{x}(-(t-t_0))$, and return exactly to their initial points after one period: there is no room for any nontrivial advection.

In order to estimate the size of the different terms in the Navier-Stokes equation (1) we take a length scale L characteristic of the spatial variations of the forcing and f_0 (with the dimensions of an acceleration) as a measure of the driving strength. In addition, we have the external frequency ω. The amplitude of the velocity field U_0 follows from the balance of forces, and will be a function of these external parameters. The size of the various terms in the Naviers-Stokes equation then is

$$\partial_t \mathbf{u} + (\mathbf{u}\cdot\boldsymbol{\nabla})\mathbf{u} = -\boldsymbol{\nabla} p + \nu\boldsymbol{\Delta}\mathbf{u} + \mathbf{f}(\mathbf{r},t)$$

$$\omega U_0 \quad U_0^2/L \quad U_0^2/L \quad \nu U_0/L^2 \quad f_0 \tag{5}$$

Since the velocity scale will be set by f_0, the nonlinear term can be neglected if

$$U_0^2/L \ll f_0. \tag{6}$$

With this term (and the pressure) gone, three terms are left and there are two ways to balance the forcing f_0: In the high frequency limit one can expect the time derivative to dominate, in which case the velocity can be estimated to be $U_0 \approx f_0/\omega$ and the condition (6) that the inertial term can be neglected becomes $f_0 \ll L\omega^2$. In the low frequency limit the forcing is balanced by the viscous term, the velocity becomes $U_0 \approx L^2 f_0/\nu$, and the condition (6) reads $f_0 \ll \nu^2/L^3$. The crossover between high and low frequencies occurs when the frequency equals the viscous damping, i.e., for $\omega \approx \nu/L^2$. Note that the Reynolds number, the ratio between the nonlinear and viscous term, is $\mathrm{Re} = f_0 L/\nu\omega$ in the high

TABLE I. Characteristic quantities for low frequencies ($\omega < \nu/L^2$) and for high frequencies ($\omega > \nu/L^2$). The velocity scale U_0 is determined as described in the text, f_{max} is the maximal amplitude from the estimate (6), $\mathrm{Re}=U_0L/\nu$ is the Reynolds number, and Re_{max} the maximal Reynolds number for maximal driving amplitude f_{max}. The Strouhal number St is inversely proportional to the driving amplitude f_0 and will diverge for small amplitudes. Note that in the high frequency case the Reynolds number increases linearly with frequency and can become large without the nonlinear terms becoming important.

	Low ω	High ω
U_0	f_0L^2/ν	f_0/ω
f_{max}	ν^2/L^3	ω^2L
Re	f_0L^3/ν^2	$f_0L/\omega\nu$
Re_{max}	1	$\omega L^2/\nu$
St	$\omega\nu/(f_0L)$	ω^2L/f_0

frequency limit and $\mathrm{Re}=f_0L^3/\nu^2$ in the low frequency limit: in both cases it is proportional to the amplitude of the driving and can be made arbitrarily small for weak driving.

In connection with periodic driving often the Strouhal number $\mathrm{St}=L\omega/U_0$ is used. It measures the importance of the time derivative relative to the nonlinear term. Since we want to work in a range of forcings where we can use the linear equations the Strouhal number can become large. So if the nonlinear term is small we have small Reynolds number but large Strouhal number and a nonvanishing product of both. It should be noted, however, that the term of reference for both expressions, the nonlinear term, can be neglected for the limit of small driving that we are interested in here. We, therefore, find neither the Reynolds number nor the Strouhal number very useful in characterizations of the system for small forces f_0.

The characteristic quantities that follow from a low and a high frequency analysis are collected in Table I. For the experiments [11–13] typical numbers are $L\approx 10^{-2}$ m, $\omega \approx 1$ Hz, and $\nu=10^{-6}$ m^2/s, so that $\nu/L^2\approx 10^{-2}$ s$^{-1}\ll\omega$ and the experiments are in the high frequency regime. The velocity fields are $U_0\approx 10^{-2}$ m/s, so that the Reynolds numbers are $\mathrm{Re}\approx 100$. Nevertheless, the nonlinear terms in the Navier-Stokes equation can be neglected.

III. EIGENMODE EXPANSION

Without the inertial term the Navier-Stokes equation becomes an inhomogeneous linear differential equation and solutions can conveniently be expanded in terms of eigenmodes of the homogeneous equation. Therefore let $\mathbf{u}_\lambda$ be divergence-free velocity fields that satisfy the boundary conditions as well as

$$\Delta\mathbf{u}_\lambda = -\lambda\mathbf{u}_\lambda. \tag{7}$$

Then both the velocity field and the driving can be expanded in these modes,

$$\mathbf{u} = \sum_\lambda c_\lambda(t)\mathbf{u}_\lambda(\mathbf{x}), \tag{8}$$

and

$$\mathbf{f} = \sum_\lambda f_\lambda\mathbf{u}_\lambda(\mathbf{x}), \tag{9}$$

and the equations for the individual amplitudes become

$$\dot{c}_\lambda = -\nu\lambda c_\lambda + f_0f_\lambda e^{i\omega t}. \tag{10}$$

The solution

$$c_\lambda(t) = \frac{f_0f_\lambda}{\nu\lambda + i\omega}e^{i\omega t} \tag{11}$$

shows that each eigenmode λ responds with a delay, $c_\lambda(t) \sim \exp(i\omega t - i\delta_\lambda)$, where the phase shift is given by

$$\delta_\lambda = \mathrm{atan}\left(\frac{\omega}{\nu\lambda}\right). \tag{12}$$

This phase shift depends on the frequency of the driving and also on the relaxation damping rate $\nu\lambda$ of the eigenmode λ. If the driving has the reversal symmetry (3) and contains only a single mode, the reversal symmetry persists, but with respect to an origin of time shifted by δ_λ/ω, as allowed for in Eq. (4). But as soon as modes with different damping constants λ appear in the forcing, they will have reversal symmetry with respect to a different zero of time, and in their superposition the reversal symmetry is lost. Since the phase shifts approach zero in the limit of vanishing frequency and approach $\pi/2$ for infinite frequency this *viscous dephasing* should be strongest if the frequency of driving is compatible to the damping rates of the modes that are driven.

Should the driving couple to a single eigenmode of the system only, more general time dependencies will still give a complete reversal in the dynamics. Take a forcing of mode λ with a general time dependence $g(t)$ that need not be periodic. Then $\mathbf{f}=f_0\mathbf{u}_\lambda(\mathbf{x})g(t)$ and the equation for the velocity response becomes

$$\dot{c}_\lambda = -\nu\lambda c_\lambda + f_0g(t) \tag{13}$$

with solution

$$c_\lambda(t) = f_0\int_{-\infty}^{t} g(t')e^{-\nu\lambda(t-t')}dt'. \tag{14}$$

The equations for particles in that velocity field then become $\dot{\mathbf{x}}(t)=\mathbf{u}_\lambda(\mathbf{x}(t))c_\lambda(t)$. The time dependence on the right-hand side can be eliminated by a transformation of time, $d\tau = c_\lambda(t)dt$, whereby the equations for the trajectories become $d\mathbf{x}/d\tau=\mathbf{u}(\mathbf{x}(\tau))$. Thus particles will return to their initial conditions as long as

$$\int_{-\infty}^{\infty} c_\lambda(t)dt = 0. \tag{15}$$

Juggling around the integrals this is equivalent to

$$\int_{-\infty}^{\infty} g(t')dt' = 0, \tag{16}$$

i.e., as long as the driving integrates to zero, so does the motion of the particles.

IV. NUMERICAL EXAMPLE

The above discussion is completely general and applies to both 3D and 2D flows. The presentation for 2D flows is simplified by the introduction of stream functions for both velocity field and driving force. A detailed discussion of the relation between Lorentz force, fluid response, boundary conditions, and two-dimensionality has been given in [14]. We here assume that flow and forcing are 2D and work with stream function representations for both. With $\psi_f(\mathbf{r}) = \text{curl}\,\mathbf{f}(\mathbf{r})|_z$ and $\mathbf{u}(\mathbf{r},t) = \text{curl}(\psi(\mathbf{r},t)\mathbf{e}_z)$ the equation that has to be solved is

$$\partial_t \Delta\psi = \nu\Delta\Delta\psi - f_0\psi_f e^{i\omega t}. \tag{17}$$

In an unbounded domain the natural eigenstates are Fourier modes. In view of the cellular structures used in the experiments, we use a superposition of two modes,

$$\psi_f = k_x \sin k_x x \cos k_y y + 5k_x \sin 5k_x x \cos k_y y. \tag{18}$$

The phase delays for the two modes are $\text{atan}(\omega/\nu k_1^2)$ and $\text{atan}(\omega/\nu k_2^2)$, where $k_1^2 = k_x^2 + k_y^2$ and $k_2^2 = 25k_x^2 + k_y^2$ are the norm of the wave vectors. The phase difference $\Delta\delta = \delta_1 - \delta_2$ is maximal for $\omega = \nu k_1 k_2$, with a value $\Delta_{max} = \text{atan}[(k_2^2 - k_1^2)/(2k_2k_1)]$.

For the numerical simulations we take $k_x = 1$ and $\nu = 1$ and $k_y = \sqrt{2}$. The eigenvalues of the Laplacian for the modes then are $\lambda_1 = 3$ and $\lambda_2 = 27$ and the stream function of the resulting velocity field is

$$\psi = \frac{f_0}{3\sqrt{9+\omega^2}} \sin(\omega t - \delta_1)\sin x \cos\sqrt{2}y + \frac{5f_0}{27\sqrt{729+\omega^2}} \sin(\omega t - \delta_2)\sin 5x \cos\sqrt{2}y. \tag{19}$$

The phase delays are $\delta_1 = \text{atan}(\omega/3)$ and $\delta_2 = \text{atan}(\omega/27)$. Their difference vanishes for low frequencies, becomes extremal for $\omega_m = 9$ and decays slowly towards zero again for high frequencies. Isocontours of the instantaneous stream function at times when only one mode is present are shown in Fig. 1. These differences in the instantaneous flow field drive the chaotic advection.

The velocity field preserves the symmetry lines $x = 0$, $x = \pi$, and $y = \pm\pi/2\sqrt{2}$ so that no particles can cross between cells. The dimension of this fundamental cell is a quarter of the period box, which has lengths $2\pi \times 2\pi/\sqrt{2}$. The four copies of the fundamental domain that fit into the period box differ only in orientation of the vortices: the one to the right and above has negative ψ and thus an opposite sense of rotation, and the one along the diagonal has the same sign and the same sense of rotation. The images of particle dynamics in the fundamental domain can thus be extended in a checkerboardlike pattern throughout the plane.

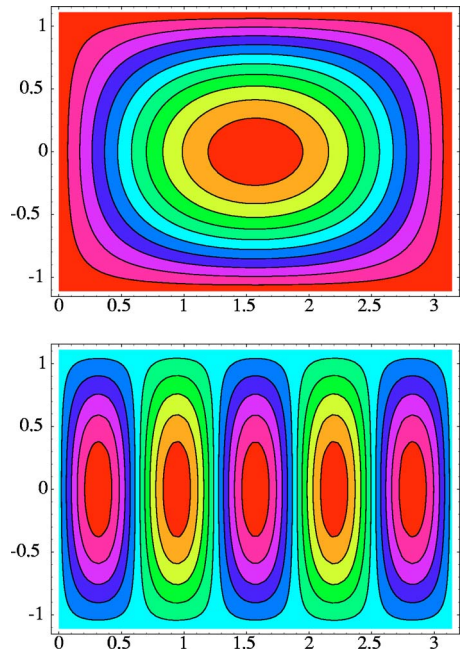

FIG. 1. (Color online) Isocontours of the instantaneous stream functions for the two eigenmodes used in the numerical simulations. Only the fundamental cell $0 < x < \pi$ and $|y| < \pi/2\sqrt{2}$ is shown. The gray shading in the top frame corresponds to one sense of orientation. The lighter and darker shades in the bottom frame indicate vortices of different orientations.

To map out the dynamics we use the stroboscopic records of the position after full periods of the driving. Figure 2 shows such stroboscopic surfaces of section for different driving amplitudes f_0. The breaking of reversal symmetry is

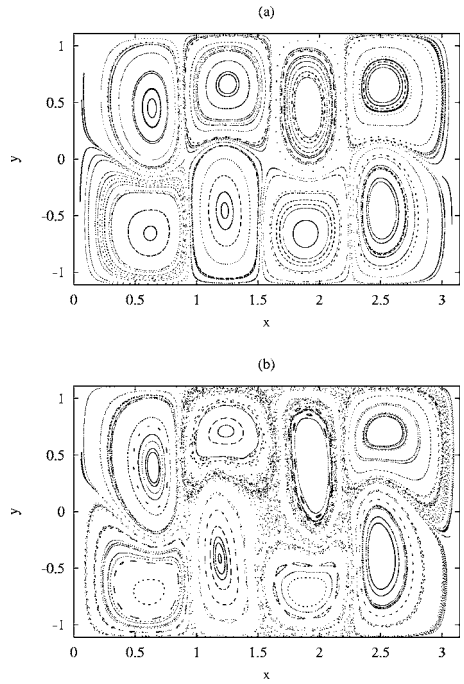

FIG. 2. Surfaces of section for 100 different initial conditions followed for 200 periods of the driving. The amplitudes f_0 of the forcing are (a) 600 and (b) 1000. The frequency is $\omega = 40.0$.

evident already for the weakest driving shown, $f_0=600$: the particles do not return to their starting point but trace out tori. As the driving increases small regions of chaotic motions appear near the separatrices between the tori, and within the tori chains of resonances form. For larger driving the chaotic regions grow and overlap to form a chaotic sea that covers almost all of the fundamental cell. While general time dependent stream functions can give chaotic motions it is interesting to note that the pattern of motions does not resemble anything of the underlying velocity field. For instance, the stream function has a local extremum for all times at $x=\pi/2$, $y=0$. However, in the final pattern this point is not an elliptic fixed point but a hyperbolic one. The transition comes about through a parametric resonance.

We have studied various combinations of wave vectors and frequency and found the high frequency case with flows of comparable amplitude to be most favorable for the appearance of chaos. The scenario for the transition to chaos seems compatible with Kolmogorov-Arnold-Moser (KAM) theory, where tori with rational winding numbers break up first and those with irrational winding numbers survive until the perturbations reach a certain strength. However, in order to formally connect it to KAM theory a zeroth order stream function that does not correspond to trivial reversible dynamics has to be identified.

The experiments [11–13] could allow experimental tests of the theory. Perhaps the most accessible prediction is the phase difference between forcing and response, that should show up in Fourier decompositions of the velocity field. This indicator is then fairly independent of uncertainties that come from the spatial dependence of the magnetic fields and are possible in the presence of inertia. Further tests could be based on modifications of the driving protocol, allowing for a transition from sinusoidal, reversible driving to asymmetric irreversible drivings. The latter may be realized with a constant offset to the sinusoidal driving or additions of terms like $\cos 2\omega t$. For theoretical discussions the constant offset has the advantage that it connects immediately to a KAM type scenario, with the constant current stream function as the unperturbed Hamiltonian and the periodic modulation as perturbation.

Nontrivial advection by a nonreversible flow despite a reversible driving is a fairly general phenomenon in driven Stokes flows. It occurs, for instance, also near a periodically oscillating sphere. The presence of large scale advection patterns can enhance particle dispersion, even before the onset of chaos (as observed, e.g., in studies in cellular Rayleigh-Bénard convection [15]). Outside the experiments that triggered this study, the relevant frequency and amplitude range seems to be most easily realized in biological situations such as the flows around oscillating flagellae or in micro- and nano-mechanical devices.

ACKNOWLEDGMENTS

This work was supported by the EU within the Network Nonideal turbulence, HPRN-CT-2000-00162. We would like to thank J.P. Gollub and G. Voth for stimulating discussions.

[1] G. M. Homsy *et al.*, *Multi-Media Fluid Mechanics* (Cambridge University Press, Cambridge, 1999).
[2] H. Aref, J. Fluid Mech. **143**, 1 (1984).
[3] H. Aref, Phys. Fluids **14**, 1315 (2002).
[4] J. M. Ottino, *The Kinematics of Mixing* (Cambridge University Press, Cambridge, England, 1989).
[5] *Symposium on Fluid Mechanics of Stirring and Mixing*, edited by A. Acrivos, H. Aref, and J. M. Ottino [Phys. Fluids **3**, Part 2 (1991)].
[6] *Chaos Applied to Fluid Mixing*, edited by H. Aref [Chaos, Solitons Fractals **4**, 745 (1994)].
[7] J. Chaiken, R. Chevray, M. Tabor, and O. M. Tan, Proc. R. Soc. London, Ser. A **408**, 165 (1986).
[8] W. L. Chien, H. Rising, and J. M. Ottino, J. Fluid Mech. **170**, 355 (1986).
[9] J. M. Ottino, Annu. Rev. Fluid Mech. **22**, 207 (1990).
[10] T. H. Solomon and I. Mezić, Nature (London) **425**, 376 (2003).
[11] Benjamin S. Williams, D. Marteau, and J. P. Gollub, Phys. Fluids **9**, 2061 (1997).
[12] D. Rothstein, E. Henry, and J. P. Gollub, Nature (London) **401**, 770 (1999).
[13] G. A. Voth, T. Saint, G. Dobler, and J. P. Gollub, Phys. Fluids **15**, 2560 (2003).
[14] B. Jüttner, D. Marteau, P. Tabeling, and A. Thess, Phys. Rev. E **55**, 5479 (1997).
[15] T. H. Solomon and J. P. Gollub, Phys. Rev. A **38**, 6280 (1988).